Polymer Chemistry

ROYAL SOCIETY OF CHEMISTRY

PAPER

View Article Online
View Journal | View Issue

Check for updates

Cite this: *Polym. Chem.*, 2024, **15**, 2308

Alkaline stability of pendant C2-protected poly(imidazolium)s†

Kate Fraser,‡ Anastasiia Konovalova, ‡ Thomas Skalski, Simon Cassegrain and Steven Holdcroft *

Received 4th March 2024,
Accepted 14th May 2024

DOI: 10.1039/d4py00235k

rsc.li/polymers

Non-fluorinated anion exchange polymers with sufficient ion exchange capacity, mechanical integrity and hydroxide-ion stability are required for the progression of alkaline electrochemical energy conversion devices. In this work, we present a new class of polycations, that possess C2-sterically protected imidazolium pendant groups which are incorporated *via* an olefinic backbone, and a synthetic route that requires no post-functionalization. The versatile 5-step synthetic route is a platform for future modifications of this family of C2-protected imidazolium-functionalised ion conducting polymers. Hydroxide-promoted degradation studies, along with DFT calculations, predict the robustness of polymers, with the benzyl-modified, C2-sterically protected imidazolium group showcasing a 8000 h half-life in 3 M NaOD/CD_3OD/D_2O at 80 °C. A humidity cycling degradation protocol, exposing the polymers to as low as 10 % relative humidity at 80 °C was implemented to reveal the relative chemical (in)stabilities of the polymers in extreme caustic conditions under accelerated timeframes.

Published on 16 May 2024. Downloaded on 3/7/2026 1:23:47 AM.

Introduction

The versatility of ion conducting polymers with the ionic functionalities as pendant groups have gained attention in the fields of polymer and materials science.[1,2] Pendant-like structures with the ionic groups bound as side chains to a polymer backbone enables tuneability of the desired material,[1] and are often used in electrochemical conversion devices due to their high ionic conductivity.[2,3]

In pursuit of a net-zero emissions goal, considerable effort has been invested into the development of renewable energy technologies such as water electrolysers, redox flow batteries, and fuel cells.[4] Many of these electrochemical systems are dependent on ion conducting polymers for the transport of mobile charged species. Ion conducting polymers can be implemented within electrochemical devices as electrolytic membranes, providing ion transport between electrodes, whilst maintaining electrical insulation; and as an ionomer, binding components of catalyst layers, and improving ion transport between active sites, as well as between the membrane and electrodes. More recently, insoluble ion conducting polymer particles have been explored as additives within catalyst layers to promote ion conduction and improve the mass transport within the device.[5–7]

Proton exchange membrane fuel cells (PEMFCs) have been actively developed over the past few decades. However, the cost of platinum group metal (PGM) catalysts and corrosion-resistant components have proved to be significant roadblocks for widespread implementation of this technology.[8,9] Moreover, the European Union recently proposed to ban per- and polyfluoroalkyl substances (PFAS), that are critical for the high performance of commercial PEMFC devices. Pendant group ion conducting polymers based on poly(phenylenes)[10,11] and poly(aryl sulfones)[12] have thus been incorporated into PEMFCs and shown to provide sufficient proton conductivity, but still require PGM catalysts.

Anion exchange membrane fuel cells (AEMFCs) offer distinct advantages over PEMFCs; namely, the ability to use non-PGM catalysts and alkaline, PFAS-free, hydroxide-conducting polymers.[9] Due to the high pH local environment, ion conducting polymers in AEMFCs require different backbone chemistry and pendant groups than PEMs. Backbones with heteroatoms linkages, such as ethers and sulfones are shown to be unstable in alkaline conditions, especially when coupled with an electron-withdrawing cationic group.[13–15] Polyolefinic backbones have been reported to possess enhanced stability to hydroxide attack, even with cationic pendant groups.[13] Polyolefinic backbones are particularly interesting due to the versatile synthetic routes available, which include atom transfer radical polymerisation (ATRP),[16] reversible addition–fragmentation chain transfer (RAFT),[17] nitroxide-mediated poly-

Department of Chemistry, Simon Fraser University, 8888 University Drive, V5A 1S6 Burnaby, British Columbia, Canada. E-mail: holdcrof@sfu.ca

†Electronic supplementary information (ESI) available. See DOI: https://doi.org/10.1039/d4py00235k

‡These authors contributed equally.

This journal is © The Royal Society of Chemistry 2024

Published on 16 May 2024. Downloaded on 3/7/2026 1:23:47 AM.

merisation,[18] Ziegler–Natta polymerisation[19] and radical chain growth polymerisation. Pendant cations groups required for ion conductions are installed onto these polymers through post-functionalisation step, where the degree and location of such groups can be challenging to control.[14,20]

Hydroxide conducting cationic groups for AEMs have been thoroughly investigated. Cations include quaternary ammonium,[21–23] cyclic ammoniums,[24,25] phosphonium,[26,27] guanidinium,[28] benzimidazolium,[29–31] and imidazolium.[29,32–34] All of these cations have been studied with respect to their alkaline stability.[35,36] Confined piperidinium cations have been identified as a group with enhanced alkaline stability,[21,37] as have imidazolium cations with steric protection around the electrophilic C2 position.[32–34] When incorporated into the polymer backbone in the form of an ionene,[32,34] poly(imidazolium)s exhibit high conductivity and mechanical strength for integration into alkaline devices.[38]

Despite their incorporation into ionenes, highly stable C2-protected imidazoliums have yet to be employed as a pendant group on polyolefins: synthetic strategies have not been proven nor has the stability of pendant C2-protected imidazoliums been examined. In this work, we studied the synthesis of C2-protected imidazoliums bound to a polystyrene backbone. A free-radical initiated chain growth polymerisation route was designed to yield poly(vinyl C2-protected imidazoliums) without the requirement of additional a post-functionalisation. Through accelerated, hydroxide-promoted degradation studies, we identify the stability against caustic solutions for this new class of polymer, and describe future work required to render these materials suitable for alkaline electrochemical energy conversion devices.

Experimental

Materials

Ammonium acetate (crystals, ACS reagent), diethyl ether anhydrous (Et_2O, ACS reagent), sodium chloride (NaCl, ACS reagent), and dimethylformamide (ACS reagent) were sourced from ACP Chemicals Inc., Canada and used as received. Acetone (ACS reagent), dichloromethane (DCM, ACS reagent, stabilized), methanol (MeOH, reagent grade), anhydrous magnesium sulfate ($MgSO_4$, certified powder), *n*-butyl bromide (certified), iodomethane (99%, stabilized with copper), hydrogen bromide, 33% w/w (45% w/v) soln. in acetic acid, and paraformaldehyde (97%), mesitylene (98+%) were sourced from ThermoFisher Scientific, USA and used as received. Benzyl bromide was purchased from Mallinckrodt Inc., USA and used as received. Benzil (98%) was purchased from Combi-Blocks Inc., USA and used as received. 2,2′-Azobis(2-methylpropionitrile) (AIBN, 98%), 1-*N*-methyl-2-pyrrolidone (anhydrous, 99.5%), ethyl-bromide (98%, reagent grade), 4-chloromethyl styrene (90%), acetic acid (ACS reagent, >99.7%), aniline (Reagent plus® 99%), acetonitrile for HPLC, gradient grade (>99.9%), hexanes, mixture of isomers (ACS reagent, >98.5%), methanol-d_4 (D, 99%), sodium deuteroxide (D, 99%), deuterium oxide (D, 99%) were purchased from Millipore Sigma Canada Co., Canada and were all used as received. Chloroform ($CHCl_3$, ACS reagent), dimethyl sulfoxide (DMSO, ACS grade), and sodium hydroxide (NaOH, ACS grade) were purchased from VWR Chemicals BDH, USA. Potassium hydroxide (KOH, reagent grade, min 85%) and tetrahydrofuran (THF, ACS grade) were sourced from Caledon Laboratories, Canada. Dimethylsulfoxide-d6 (D, 99.9%), acetone-d6 (D, 99.9%), methylene chloride-d_2 (D, 99.8%, CD_2Cl_2), and chloroform-d ($CDCl_3$, 99%) were purchased from Cambridge Isotope Laboratories Inc., USA.

Instruments

^{1}H and ^{13}C NMR spectra were recorded on a Bruker AVANCE III 500 MHz equipped with a 5 mm TXI Inverse probe at room temperature (T = 298 K) and Bruker 600 Hz QCI (Bruker Corp., USA). The following terms are defined: *s* for singlet, *d* for doublet, *t* for triplet, *q* for quadruplet and *m* for multiplet. Chemical shifts are reported in ppm and *J*-couplings are reported in Hz. Residual proton and carbon peaks for deuterated solvents were set at, respectively, 2.05 ppm and 29.84 ppm for d_6-acetone, 2.50 ppm and 39.52 ppm for d_6-DMSO, 5.32 ppm and 54.00 ppm for CD_2Cl_2, 7.26 ppm and 77.16 ppm for $CDCl_3$.

Mass spectra were recorded on an AB Sciex 4000 Q TRAP spectrometer (Danaher Corp., USA) and a Bruker MicrOTOF (Bruker Corp., USA) in both positive and negative electrospray ionization modes for ionic compounds. High accuracy mass measurements were obtained on an LC-TOF instrument (Agilent Technologies, Inc., USA) in positive atmospheric-pressure photoionization (APPI) mode. Molecular ions [M]+ was used for empirical formula confirmation.

Elemental analysis data were collected on an EA CHN 110 instrument (Thermo Fisher Scientific Inc., USA) under an O_2 atmosphere up to 960 °C. Thermogravimetric Analysis was performed on a Shimadzu TGA-50 series (Shimadzu Corp., Japan). The samples were heated from ambient temperature to 450 °C at a heating rate of 10 °C min^{-1} under constant N_2 flow. Dynamic Vapor Sorption (DVS) measurements were performed on a DVS Adventure humidity chamber and Ultrabalance (Surface Measurement Systems Ltd, UK).

Synthesis

Synthesis of 2-mesityl-3,4,5-triphenyl-imidazole (5a). To a 1 L, 2-necked round bottom flask, equipped with a magnetic stirrer, reflux condenser, and thermometer, benzil (19.99 g, 1.000 eq., 93.2 mmol) was added, along with 2,4,6-trimethylbenzaldehyde (14.38 g, 14.30 mL, 1.020 eq., 95.1 mmol), ammonium acetate (59.22 g, 8.000 eq., 745.8 mmol), aniline (53.14 g, 51.99 mL, 6 eq., 559 mmol) and glacial acetic acid (0.7 L). The reaction was refluxed for 24 h and then cooled to room temperature. The reaction mixture was precipitated into water (4 L) and left to stir for 2 h. The precipitate was recovered using vacuum filtration, washed with water (2 × 200 mL), and dried in the vacuum oven at 50 °C overnight. The precipitate was then stirred in hexanes for 2 h, filtered, and air dried. The

Published on 16 May 2024. Downloaded on 3/7/2026 1:23:47 AM.

product was obtained as a white solid (35.30 g, 91.3%, 85.2 mmol).

^{1}H NMR (500 MHz, CD_2Cl_2) δ (ppm): 7.58 (d, J_d = 7.59 Hz, 2H), 7.12–7.27 (m, 11H), 6.91 (d, J_d 7.64 = Hz, 2H), 6.83 (s, 2H), 2.25 (s, 3H), 2.11 (s, 6H).

^{13}C NMR (125 MHz, CD_2Cl_2) δ (ppm): δ 147.05, 139.37, 138.84, 138.13, 137.11, 135.57, 131.65, 131.60, 131.57, 129.55, 128.97, 128.93, 128.68, 128.57, 128.34, 128.15, 127.76, 127.61, 126.85, 21.44, 20.52.

HRMS (m/z): $[M + H]^+$ calculated for $C_{30}H_{26}N_2$: 414.2096 found: 415.2284.

Synthesis of 2-mesityl-4,5-diphenyl-1*H*-imidazole (5b). To a 3 L, three-neck round bottom flask equipped with a mechanical stirrer, a reflux condenser, and a thermometer, benzil (245.57 g, 1.000 eq., 1.137 mol) was added, followed by 2,4,6-trimethylbenzaldehyde (172.86 g, 172 mL, 1.005 eq., 1.143 mol), ammonium acetate (471.72 g, 9.000 eq., 10.24 mol) and glacial acetic acid (1.3 L). The reaction mixture was heated to reflux for 24 h then cooled to room temperature and poured into DI water (16 L) creating a white precipitate. The beakers were left to stir for 2 h, and the solid was recovered by vacuum filtration and washed with water (2 × 500 mL), then dried under vacuum at 50 °C overnight. The precipitate was then stirred in hexanes for 2 h. The solid was recovered by vacuum filtration, air dried and used without further purification. The product was a white solid (311.24 g, 80.9%, 0.920 mol).

^{1}H NMR (500 MHz, DMSO-d_6) δ (ppm): 12.33 (s, 1H), 7.56 (d, J_d = 7.40 Hz, 2H), 7.47 (d, J_d = 7.82 Hz, 2H), 7.39 (t, J_t = 7.32 Hz, 2H), 7.29 (m, 3H), 7.20 (t, J_t = 7.20 Hz, 1H), 6.98 (s, 2H), 2.30 (s, 3H), 2.18 (s, 6H).

^{13}C NMR (125 MHz, DMSO-d_6) δ (ppm): 145.00, 137.81, 137.59, 136.08, 135.63, 131.33, 128.94, 128.62, 128.10, 127.89, 127.75, 127.26, 127.12, 126.47, 126.26, 20.75, 19.99.

HRMS (m/z): $[M + H]^+$ calculated for $C_{24}H_{22}N_2$: 338.4449, found: 339.1851.

General synthesis of compounds 6b–d. In a 500 mL round bottom flask, equipped with a magnetic stirrer, compound **5b** (15.0802 g, 1.0 eq., 43.7 mmol) was dissolved in DMSO (5 mL per 1.0 mmol of **5b**). The solution was stirred for 20 min, then KOH (60 mL, 5.0 mol L^{-1}) was added dropwise. The reaction vessel was closed and left to stir for 20 min. Compound R–X (Fig. 1, 1.2 eq.) was added dropwise over 5 min. The reaction was left to stir at room temperature for 16 h. The reaction mixture was precipitated into water (1 L) and left to stir for 1 h. The white precipitate was recovered using vacuum filtration and washed twice with water (2 × 200 mL). The product was collected, stirred in methanol over 16 h, recollected using vacuum filtration and dried under vacuum at 50 °C overnight.

General synthesis of compounds 7a–d. In a 100 mL round bottom flask compound **2a–d** (1.00 eq.) was dissolved in 25 mL of acetonitrile. Benzyl bromide (1.10 eq.) was added to the reaction and the vessel was heated to 80 °C for 24 h. After cooling, the reaction mixture was precipitated in 150 mL of ethyl acetate, filtered under vacuum, and rinsed with 10 mL of ethyl acetate. The compound was dried in the oven at 80 °C for 16 h. The compounds were obtained as pale grey powders.

General synthesis of compounds 8a–b. In a 100 mL round bottomed flask, compounds **2a–d** (1.0 eq.) were dissolved in acetonitrile (100 mL). Chloromethyl styrene (1.15 eq.) was added dropwise, and the reaction was heated to 80 °C for 24 h. After cooling, the reaction mixture was precipitated in 150 mL of ethyl acetate, filtered under vacuum, and rinsed with 10 mL of ethyl acetate. The compounds was dried in the oven at 80 °C for 16 h. The compounds were a white powder.

Synthesis of Poly(Styrene Mesityl-Imidazolium) PSMI-Ph-[Cl$^-$] and PSMI-Bn-[Cl$^-$]. In a 16 mL Schlenk tube, compound

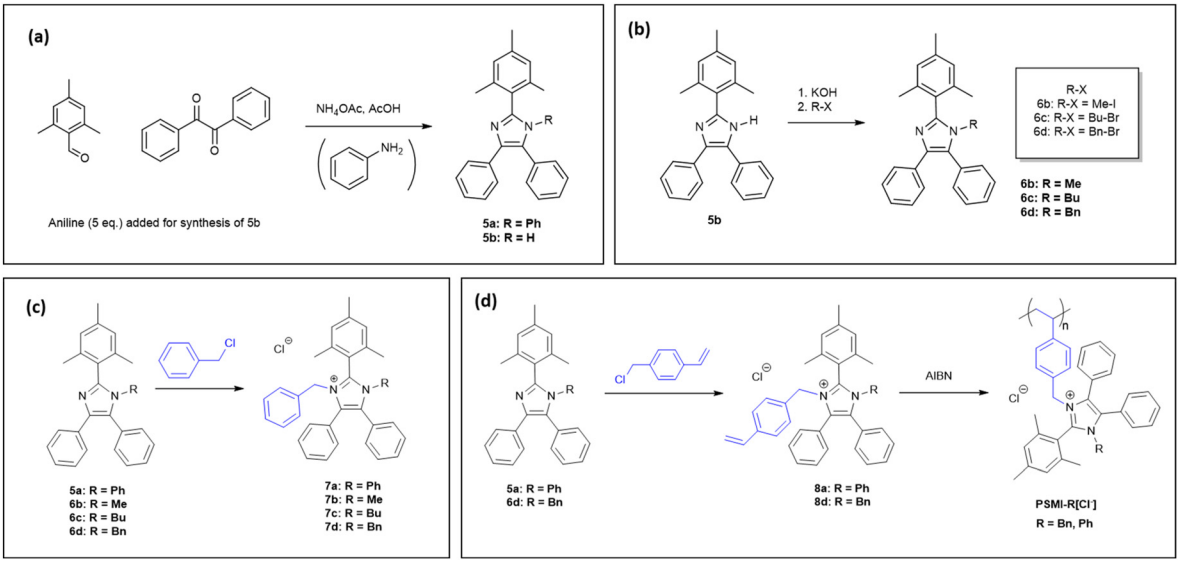

Fig. 1 (a) Synthesis of imidazole monomer precursors (b) first *N*-functionalisation step (c) second *N*-functionalisation step for synthesis of imidazolium model compounds (d) second *N*-functionalisation for monomer synthesis followed by polymerisation.

 This journal is © The Royal Society of Chemistry 2024

Published on 16 May 2024. Downloaded on 3/7/2026 1:23:47 AM.

4 (1.00 eq.) was dissolved in NMP (2.5 mL), and AIBN (0.01 eq.) was added. The Schlenk reaction was freeze–pump–thawed four times, to replace the atmosphere with argon. The reaction was heated at 80 °C for 5 days. After cooling, the polymers were precipitated into ice cold water and stirred for 1 h. The precipitates were recovered as fine powders and dried in the oven overnight.

Characterisation

DFT calculations. Electronic structure calculations were performed using Gaussian G09, B3LYP density functional theory (DFT). Pre-optimisation was performed using the 6-31G(d) basis set and final calculations were performed using the 6-311++G(2d,2p) basis set.[30,32] Vibrational frequency calculations at the same level of theory were performed at 298.15 K. The Polarisable Continuum Model (PCM) was used for implicit solvent using the G09 integrated integral equation formalism (IEFPCM) with water as solvent (ε = 78.36).

Solution degradation studies. Carried out directly in sealed NMR tubes with valves to avoid transfer inconsistencies, 17 mg of each model compound (**7a**, **7b**, **7c**, **7d**) were dissolved in 0.5 ml of methanol-d_4 (Table 1). Sodium deuteroxide was added accordingly to reach the desired molar concentration of the alkaline solution. Solution concentrations were 1, 3, 5, and 7 M $NaOD/CD_3OD/D_2O$. Tightly closed NMR tubes with valves containing experimental solutions were exposed to 80 °C in the oven for up to one month. The evolution of NMR spectra over time was compared with an original spectrum of a compound immediately after contact with caustic solution. All ^{1}H NMR data were recorded on a Bruker 600 Hz QCI. Number of scans 16.

Ionic conductivity. Prior to measurement, PSMI-**Bn** sample was submerged into 3 M NaCl (aq.) for 24 hours followed by a subsequent submersion in DI water to remove excess chloride ions. The chloride conductivity of polymer compound PSMI-**Bn** was measured by compressing a given quantity of polymer powder between two stainless steel rods tipped with Pt disks electrodes inside a 0.58 cm diameter glass tube (Fig. S1†). The thickness of the circular pellet of powder (approximately 2–3 mm) was measured with a digital caliper after the experiment to record a humidified thickness value. The cell was kept compressed in a clamp during the measurement to ensure proper contact between the components. Electrochemical Impedance Spectroscopy (EIS) was performed over the frequency range of 10 MHz to 100 Hz with 100 mV amplitude. Prior to the data collection, the cell was equilibrated at 80 °C at 95 % relative humidity (RH) in an environmental chamber (SH-241, ESPEC North America Inc.) for 5–6 hours. The ionic conductivity σ [Ohm cm^{-1}] was calculated using eqn (1), where L [cm] is the thickness of the pellet, A [cm^2] is its surface area, and R [Ohm] is the measured resistance.

$$\sigma = \frac{L}{R \cdot A} \tag{1}$$

Water uptake and hydration number. PSMI-**Bn** polymer was dried in a vacuum oven (80 °C, 24 h) and the dry mass m_{dry} [g] of the sample was recorded in the dynamic vapor sorption (DVS) instrument at the initial step of the procedure. The humidity was controlled by a source of deionized water delivered under nitrogen gas flow at a volumetric flow rate of 200 (sccm). The sample was held at a constant temperature of 80 °C and absorption curve was recorded under 85 %RH to collect humidified mass m_{wet} [g] of the sample. Water uptake, WU [%], was calculated according to eqn (2). The hydration number, λ, that corresponds to the number of water molecules per ion pair, was calculated from the ratio of moles of water, $n_{\mathrm{H_2O}}$/mol, per dry mass of polymer, m_{dry} [g], with respect to theoretical ion exchange capacity, *IEC* [mmol g^{-1}], as shown by eqn (3).

$$\mathrm{WU} = \frac{m_{\mathrm{wet}} - m_{\mathrm{dry}}}{m_{\mathrm{dry}}} \cdot 100\% \tag{2}$$

$$\lambda = \frac{n_{\mathrm{H_2O}}}{\mathrm{IEC} \cdot m_{\mathrm{dry}}} \tag{3}$$

The theoretically derived IEC value was calculated using eqn (4), where M (PSMI-Bn) [mol g^{-1}] is a molar mass of PSMI-**Bn** polymer and M (OH^-) [mol g^{-1}] is a molar mass of hydroxide ion and equals 1.7 mmol g^{-1}.

$$\mathrm{IEC}_{\mathrm{teor,OH^-}} = \frac{1}{M(\mathrm{PSMI\text{-}Bn}) + M(\mathrm{OH^-})} \tag{4}$$

Polymer degradation studies. Alkaline degradation of polymers was investigated by DVS consisting of equilibration of the material followed by cycling between 70 %RH and 10 %RH. The mass of the sample was monitored during the collection of water adsorption and desorption curves. The amount of water absorbed directly correlates with hydration of the sample that is rapidly decreasing under dry hydroxide-saturated conditions and correlates to the number of available ionic sites. Prior to the degradation study, polymer PSMI-**Bn** was exchanged to OH^- form by submersion into 3 M KOH (aq.) for 24 hours followed by a subsequent submersion in DI water to remove excess hydroxide-ions. The sample was kept under the water until the transfer to the platinum boat of DVS instrument to avoid contamination. The glassware was thoroughly flushed with N_2 gas before the use and the powder transfer was performed under the glass dome cover filled with the inert gas to minimize cross contamination with CO_2 found in the atmosphere. After the sample was loaded into the instrument, a calibration was performed at 85 %RH to stabilize the mass of the sample. Relative humidity was cycled from

Table 1 Molar concentration of compounds **7a–7d** in alkaline solutions used for the degradation test

Compound, M (g mol^{-1})	Molar concentration, mol l^{-1}
7b, 443.61	0.077
7c, 485.69	0.070
7a, 505.68	0.067
7d, 519.71	0.065

Published on 16 May 2024. Downloaded on 3/7/2026 1:23:47 AM.

high to low seven times. The change in mass and theoretical IEC was used to calculate hydration number of the polymer at a given step according to eqn (3). Proportionally, the change in hydration number corresponds to the change in IEC from which the percentage of degradation was estimated.

Results

Compound **5a** was synthesised *via* a 4-component condensation route, using benzil, trimethylbenzaldehyde, ammonium acetate, and an excess of aniline (Fig. 1a). Compound **5b** was synthesised *via* a 3-component (benzil, trimethylbenzaldehyde, and ammonium acetate) condensation reaction as per previously reported in the literature (Fig. 1a).[32] **5b** was dissolved in DMSO, deprotonated with excess KOH and reacted with iodomethane, butyl-bromide or benzyl-bromide to yield the single *N*-alkylated imidazole (Fig. 1b). The *N*-functionalisation was varied to compare the impact of substituents on imidazolium stability, reactivity in the polymerisation step, and to tune the ion exchange capacity of the polymer. The second *N*-functionalisation of compounds **5a**, and **6b–d** proceeded with either benzylchloride (compounds **7a–d**, Fig. 1c) or vinyl benzylchloride (compounds **8a–d**, Fig. 1d). Fig. 2 depicts collected ^{1}H NMR spectra of a representative synthetic route **5b–6d–7d–8d**. All model compounds and monomers were characterized using ^{1}H NMR, ^{13}C NMR, and mass spectroscopy. Remaining spectral data can be found in the ESI (Fig. S2–S25†).

The dihedral angle was investigated *via* DFT calculations, using the optimized geometries of compounds **7a–d**. The dihedral angles are measured between the mesityl groups and the imidazolium ring and consist of two values dependent on which side of the mesityl-imidazolium compound was measured. It was expected that the compounds with a dihedral angle closer to 90° would have the highest C2 steric protection and therefore the highest stability with respect to hydroxide attack at the C2 position.[31] The *N*-functionalisation groups are known to have an impact on the mesityl-imidazolium dihedral angle.[31] The variation of *N*-functionalisation for compounds **7a–d** were expected to impact the dihedral angle and therefore the stability of the imidazoliums. Compound **7d** has the closest dihedral angle to 90°, followed by **7c**, then **7a** and **7b** as shown in Table 2. This suggests a stability trend as follows: **7d**

Table 2 Predicted dihedral angle values for compounds **7a–7d** from optimized geometries of DFT calculations

Compound	Dihedral angle – DFT (°)	LUMO energy (eV)
7a (Ph)	76.5/78.6	−1.51
7b (Me)	75.8/77.2	−1.45
7c (Bu)	78.5/78.7	−1.46
7d (Bn)	82.3/86.8	−1.49

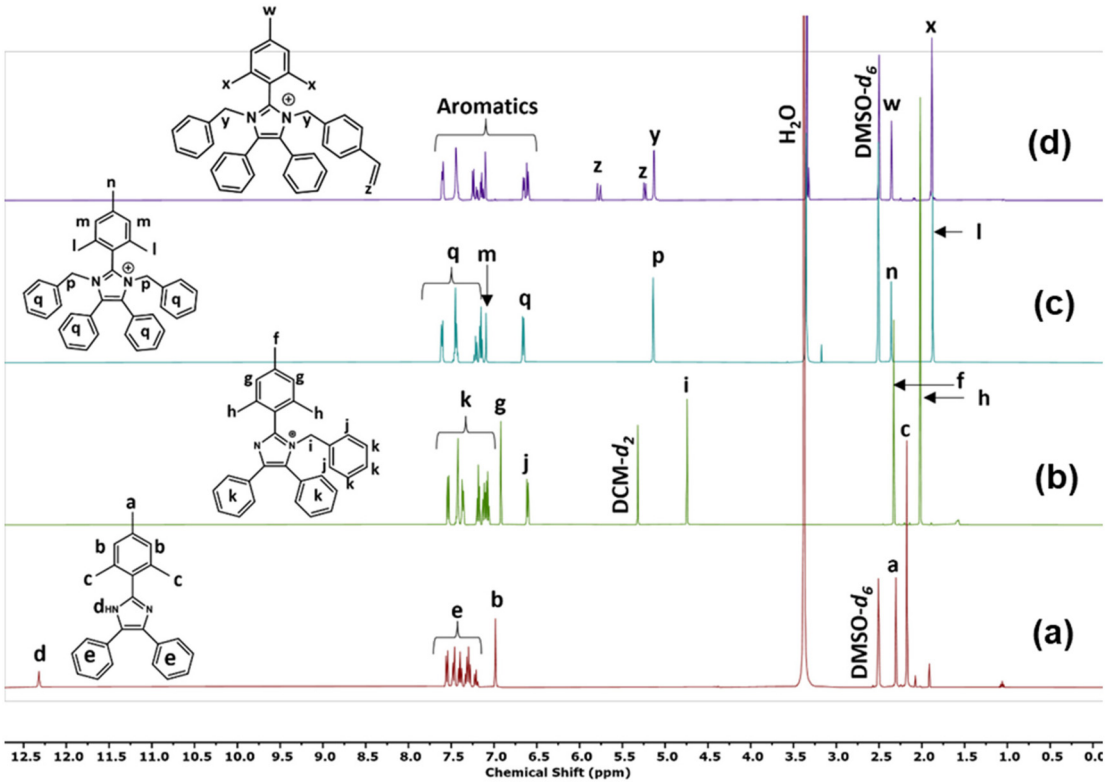

Fig. 2 ^{1}H NMR spectra of compounds (a) **5b**, (b) **6d**, (c) **7d**, and (d) **8d** confirming the synthetic route progression.

 This journal is © The Royal Society of Chemistry 2024

Published on 16 May 2024. Downloaded on 3/7/2026 1:23:47 AM.

> **7c** > **7a** > **7b**. However, this trend was not precisely observed experimentally, as illustrated below.

The hydroxide stability of imidazoliums **7a–d** were measured using the methods described by the Coates group.[39] The compounds (0.02 M) were dissolved in a mixture of 3 M NaOD in CD_3OD/D_2O, stored at 80 °C and the changes in chemical structures were monitored using ^{1}H NMR spectroscopy. Fig. 3a shows the evolution of the ^{1}H NMR spectra of compound **7d**, which was found to be the most stable molecule, over a period of 720 h. Significant deuterium exchange was observed for the –CH_2 benzyl protons at the position M, 7.1 ppm and the –CH_3 protons on the mesityl group position L, 1.75 ppm.[40] The extent of degradation was quantified by comparing the change in integration of the benzyl –C*H* protons (Fig. 3a, protons q, 6.50, 7.12, and 7.21 ppm, respectively). There was no notable ring opening degradation from hydroxide attack at the C2-position, implying the benzyl groups provided sufficient C2 steric protection, as suggested by the dihedral angles. However, chemical degradation occurred through the de-functionalisation at the imidazolium N atoms as can be seen by the reduction of the peak P at 5.2 ppm. After 720 h, only 6% of compound **7d** was degraded.

The degradation of compounds **7a–d**, monitored by ^{1}H NMR spectroscopy, was exponentially fitted to estimate the half-life ($t_{1/2}$). The remaining degree of functionalization for each molecule is shown in Fig. 4. The steric encumberment provided by the *N*-benzyl and *N*-methyl groups restricted hydroxide attack at the C2-position but the methyl group was not sufficiently bulky to prevent de-alkylation, resulting in an estimated half-life of only 852 h and over 30% of degradation after 504 h for molecule **7b**. The additional steric hindrance provided by the butyl (**7c**), phenyl (**7a**) and benzyl (**7d**) groups created a five-fold increase in stability for the molecules: half-lives of 3410, 3520 and 7730 h, respectively, with over 90% functionalization remaining after 504 h of degradation test for **7a** and **7d**.

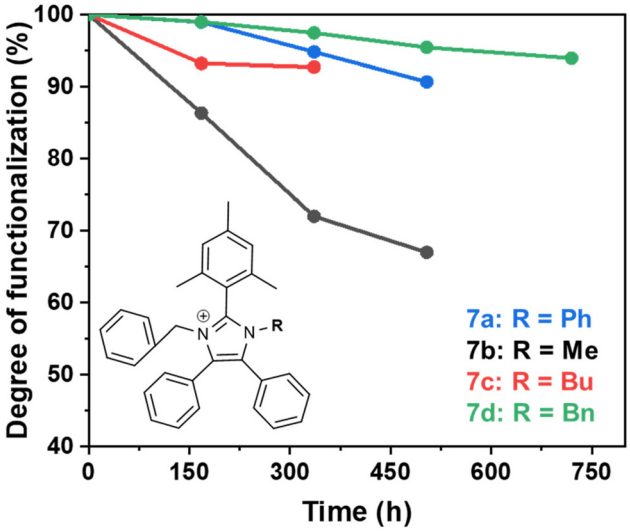

Fig. 4 The degree of functionalization remaining after the alkaline degradation test performed on synthesised molecules in 3 M NaOD/CD_3OD/D_2O at 80 °C at various intervals over 720 h.

Fan *et al.* compared half-lives of various imidazolium model compounds ranging from 1370 h to over 10 000 h. In this report, model compound **7d** (Bn) with a half life of 7730 h compares to a previously reported imidazolium cation with 7790 h half life stability evaluated under similar conditions.[32] Suggested degradation pathways of the model compounds are presented in Fig. 5 which depicts a general structure of synthesised molecules undergoing either de-alkylation *via* hydroxide attack on the benzyl methylene or a direct C2 attack followed by the ring opening.[32,34]

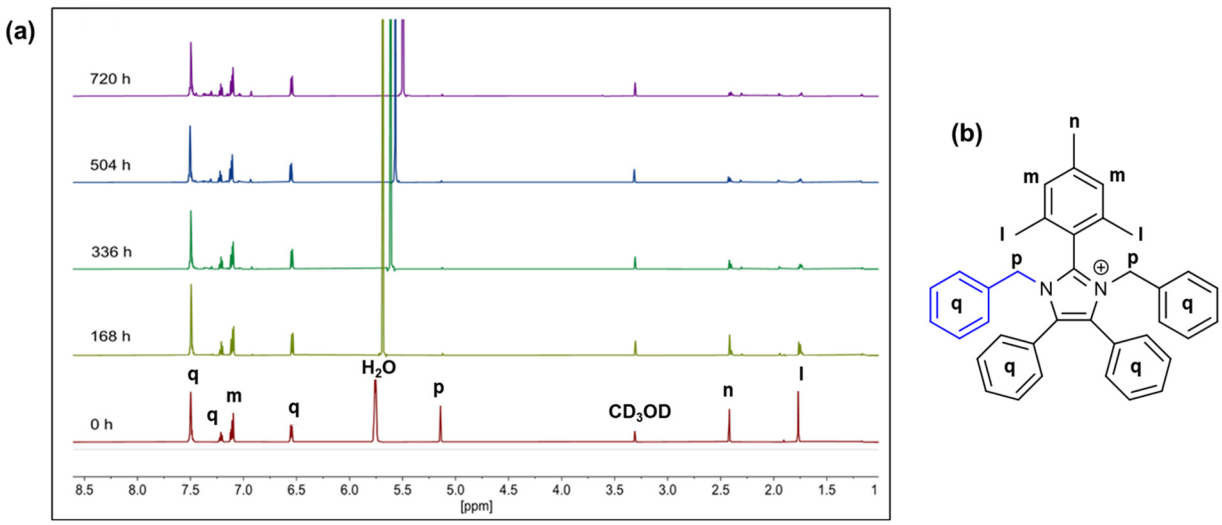

Fig. 3 (a) ^{1}H NMR of a representative compound **7d** in 3 M NaOD/CD_3OD/D_2O at 80 °C at various intervals over 720 h. (b) Proton labeling of compound **7d**.

Published on 16 May 2024. Downloaded on 3/7/2026 1:23:47 AM.

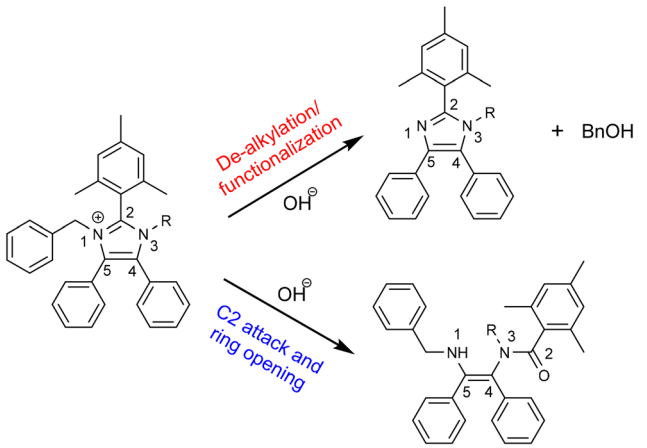

Fig. 5 Possible hydroxide degradation scheme of the analysed model compounds **7a–d**.

The experimental and theoretical dihedral angles only partially agree with the degradation test results. The theoretical results give a stability trend of: **7d** (Bn) > **7c** (Bu) > **7a** (Ph) > **7b** (Me), in comparison to the experimental results which have a trend of: **7d** (Bn) > **7a** (Ph) > **7c** (Bu) > **7b** (Me).

A common finding for both theoretical and experimental trends is that the steric hindrance of the benzyl group, **7d** exhibits an enhanced alkaline stability compared to the short alkyl chain functionalized polymer, **7b**. There is an inconsistency between compounds **7c** and **7a**, where the theoretical results predict **7a** having a lower stability than **7c**, but the experimental results found this to be the opposite. The minor discrepancy between theoretical and experimental results could be related to the fact that the dihedral angles only consider steric encumberment around the C2 position and do not account for electronic effects that also impact stability. To investigate the electronic impact of the different *N*-functionalities, the lowest unoccupied molecular orbitals (LUMOs) of compounds **7a–d** were calculated (ESI, Fig. S26 and Tables S1–S4†). The degradation reactions require the correct energy difference between the LUMO and the highest occupied molecular orbital (HOMO) of the hydroxide anion. Therefore, the lower the energy of the LUMO the more susceptible the compound is to hydroxide attack. Interestingly, the energies of the LUMOs were in the order **7b** (Me) > **7c** (Bu) > **7d** (Bn) > **7a** (Ph), which disagrees with the result obtained from the theoretical and experimental dihedral angles, and the degradation studies. However, there was very little difference in the values of the LUMOs, possibly suggesting there is a contribution from both the steric and electronic effects that impact the stability of the imidazoliums.

The high hydroxide stability of compound **7d** (Bn) and **7a** (Ph) inspired the incorporation of these C2-protected imidazoliums as potentially stable ionic groups on a polyolefinic backbone. Vinyl imidazolium monomers (**8a, d**) were polymerised using azobisisobutyronitrile (AIBN) in *N*-methyl-2-pyrrolidone (NMP) (Fig. 1d). The radical chain growth polymerisation mechanism created a polyolefin with C2-protected imidazolium pendant groups. The optimised synthesis of the PSMI-R [Cl^-] polymers was conducted using 1.00 eq. of compound **8a, d**, 0.05 eq. of AIBN, in NMP for 168 h. The polymers synthesised in these conditions were insoluble in most common organic solvents. Importantly, the design of the vinyl monomers and the polymerisation route ensured a homopolymer was synthesised with identical repeat units, each containing one imidazolium pendant group. No post-polymerisation functionalisation was required. The chemical composition of the polymers was investigated using elemental analysis and collected data is shown in Table 3.

Thermogravimetric analysis was deployed to determine the thermal stability of the synthesised polymers. TGA curves of the polymers up to 450 °C under N_2 shown in Fig. 6. Both curves display at least two distinctive steps, where the first step indicates the loss of the water trapped in the polymer and the second step reveals a thermal degradation of the olefinic polymer backbone which starts at about 350 °C.[41] The TGA analysis of PSMI-**Bn** reveals an additional degradation that can be associated with a thermal decay of the pendant benzyl group. The temperature of 200 °C, at which degradation is initiated, is much above typical operational temperatures of polymer membrane electrochemical energy conversion devices.[8,9]

Based on the liquid alkaline stability of model compounds, PSMI-**Bn** was expected to have the highest resistance to hydroxide attack and was therefore further investigated in polymer

Table 3 Elemental analysis data (theoretical and experimental)

Sample	H (%)	N (%)	C (%)
PSMI-Ph (t)	6.2	4.9	82.5
PSMI-Ph (e)	6.6	5.2	80.0
PSMI-Bn (t)	6.4	4.8	82.6
PSMI-Bn (e)	6.3	4.9	79.6

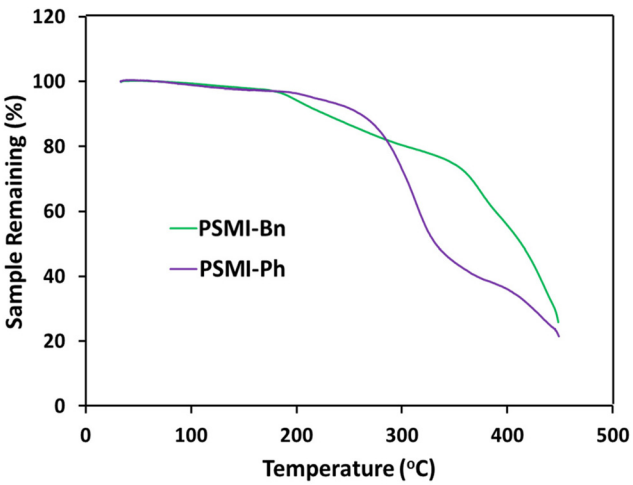

Fig. 6 TGA curves of polymers under N_2.

 This journal is © The Royal Society of Chemistry 2024

Published on 16 May 2024. Downloaded on 3/7/2026 1:23:47 AM.

form by DVS technique to determine water uptake, hydration number and hydroxide stability under low hydration conditions. The water uptake of PSMI-**Bn**[Cl^-] was determined to be 6.8 wt% at 70 %RH and 80 °C, yielding a hydration number of approximately 2. The chloride conductivity of this polymer in powder form was 1.18 mS cm^{-1} at 80 °C and 95 %RH evaluated *via* the method described by A.L.G. Biancolli *et al.*[42] Previous research shows that poly(benzimidazolium) based polymers exhibit chloride conductivity of 3–4 mS cm^{-1} under similar conditions,[43] while poly(imidazolium) based polymers in chloride-form have shown 10 mS cm^{-1}.[32] Named materials were evaluated in a free-standing film form, while ionic conductivity of PSMI-**Bn** was determined in its pelletized powder form, which contains a significant number of grain boundaries that reduces ionic conductivity. The stability of the polymer could not be investigated through a ^{1}H NMR spectroscopic analysis due to the polymer's poor solubility, so the DVS degradation protocol described by Kreuer *et al.*,[44] was employed. This method enables the stability of the polymer to be investigated in its powder form by measuring the change in water uptake whilst cycling through various levels of hydration. The hydration number (λ) of ionic polymer is correlated to its IEC at a given temperature and relative humidity (eqn (3)). Therefore, the degradation of the polymer can be investigated under controlled temperature and RH by measuring the mass loss of the sample. The mass loss of the sample occurs due to release of trapped water in the polymer structure, as the degree of functionalisation and therefore IEC of the sample is decreasing due to the degradation. The mass loss may also be exacerbated by loss of volatile degradation products, which are accounted for in this work.

Prior to the DVS measurement, the polymer sample was converted into its hydroxide form (as described in the Experimental section) and cycled from 70 %RH to 10 %RH. These conditions differ from the stability tests conducted in solvent, as described for the model compounds. The solution-based stability tests possess a much higher λ ($H_2O:OH^-$) ratio, than that under the low RH attained in this thermogravimetric method. The low hydration levels increase the reactivity of the hydroxide anion, rendering degradation much faster. The design of this method is more suitable for ion conducting polymers in AEMFC applications, since harsh hydroxide saturated conditions are mimicking drying of the cathode side of the cell caused by the electroosmotic drag of water, being especially degrading towards ionomer-binder incorporated into the catalyst layer.[45,46]

The test was conducted at 80 °C. Relative humidity of 70% was chosen as a probing humidity and it was held at intervals of 5 h, while a decomposition relative humidity of 10% was held for 10 h. As can be seen from the Fig. 7, after stabilizing the PSMI-**Bn**[OH^-] polymer sample at 85 %RH and confirming its starting weight, the humidity was lowered to initial probing humidity of 70 %RH to begin the degradation cycling. The mass of the polymer was assumed to be stable during the probing periods of 70 %RH. The hydroxide degradation was identified from the decreasing difference in hydration number at both high and low humidities, as well as the recorded decrease in mass during decomposition periods. The fast

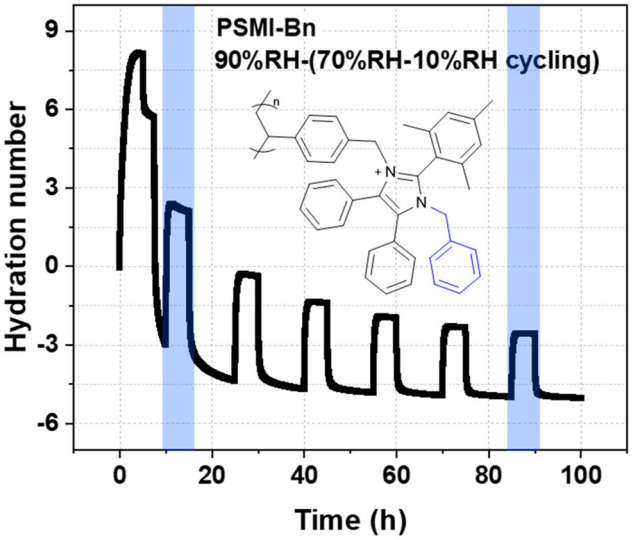

Fig. 7 DVS curve collected at 80 °C. The change in weight is monitored *via* the change in hydration number assuming a constant theoretical IEC of 1.7 mmol g^{-1}. Initial 5 h of experiment at 85 %RH was conducted to condition the polymer and collect a maximum accessible water uptake and hydration number value.

initial degradation observed during first 20 h is attributed to the harsh conditions of the test. The IEC loss estimation was calculated from the first and the last decrease in hydration number as indicated on Fig. 7. According to the calculation, the IEC of PSMI-**Bn**[OH^-] decreased by 75% of its initial IEC value over 90 h of harsh hydroxide-saturated conditions suggesting a comparable loss of the polymer's functionality.

Conclusions

For the first time, C2-protected imidazoliums were incorporated into a polyolefin backbone as pendant groups. *N*-functionalisation of the imidazoliums was used to probe the effect of steric bulk on hydroxide stability. The alkaline stability of the model compounds was assessed, using ^{1}H NMR spectroscopy, dihedral angle analysis, and LUMO energies. DFT analyses showed the phenyl and benzyl *N*-functionalities caused the C-2 attached mesityl group to lie ~90° with respect to the imidazolium ring. ^{1}H NMR spectroscopic studies corroborated these results by finding the two benzyl *N*-functionalities provided the highest protection against hydroxide degradation. The benzyl substituted model compound, **7d**, degraded only 6% after 720 h under the harsh alkaline conditions, yielding a projected half-life of 7730 h, which is at least 5 times higher than the corresponding model compound possessing a short methyl chain and 2 times higher than the rest of model compounds synthesized in this work.

Polyolefins were synthesised using a radical chain growth polymerisation mechanism. In this method, the polymerisation reaction is the only synthetic step that removes the requirement for complex post-polymerisation functionalization

Published on 16 May 2024. Downloaded on 3/7/2026 1:23:47 AM.

reactions eliminating potential batch-to-batch inconsistencies and increasing reproducibility of the synthesis. The reaction yielded insoluble polymers that were characterised using elemental and thermogravimetric analysis for chemical structure. Elemental analysis confirmed the percentage composition of the product and TGA analyses revealed two-step temperature-induced changes for PSMI-**Ph** that suggests water removal and polyolefin backbone degradation at 350 °C, while PSMI-**Bn** sample had signs of functionalization loss at 200 °C. Water uptake, hydration number and stability of the polymer samples were evaluated by DVS. Humidity cycling between 70 %RH and 10 %RH of PSMI-**Bn** [OH^-] revealed loss of polymer mass associated with loss of absorbed water (hydration number) that correlates with IEC. PSMI-**Bn**, while possessing a half-life of 7730 h in 3 M $NaOD/CD_3OD/D_2O$ at 80 °C as a model compound, lost 75% of its initial IEC value over nearly 100 h when exposed to very dry conditions (10 %RH) at 80 °C under accelerated degradation environment where λ values can become as low as 2.

While PSMI-**Bn** is the most stable of the polyolefin cationic structures studied here, the observed instability under accelerated degradation conditions provides insight into the challenges surrounding the design and synthesis of stable hydroxide ion conducting polymers under extreme caustic exposure. Nonetheless, this work presents a synthetic platform for future structural modifications of either the polymer backbone or ionic group to improve the alkaline stability of C2-protected poly(imidazolium) materials.

Conflicts of interest

There are no conflicts to declare.

Acknowledgements

This research was funded by the Natural Sciences and Engineering Research Council of Canada (NSERC) through Discovery Grant RGPIN-2018-03698. The authors gratefully acknowledge Wen Zhou, Thomas Weissbach, and Carol Wu for useful discussions and technical help with the instruments.

References

1 W. Qian, J. Texter and F. Yan, *Chem. Soc. Rev.*, 2017, **46**, 1124–1159.
2 P. Jannasch and E. A. Weiber, *Macromol. Chem. Phys.*, 2016, **217**, 1108–1118.
3 T. Ban, M. Guo, Y. Wang, Y. Zhang and X. Zhu, *J. Membr. Sci.*, 2023, **668**, 121255.
4 J. R. Varcoe, P. Atanassov, D. R. Dekel, A. M. Herring, M. A. Hickner, P. A. Kohl, A. R. Kucernak, W. E. Mustain, K. Nijmeijer, K. Scott, T. Xu and L. Zhuang, *Energy Environ. Sci.*, 2014, **7**, 3135–3191.
5 E. Balogun, S. Cassegrain, P. Mardle, M. Adamski, T. Saatkamp and S. Holdcroft, *ACS Energy Lett.*, 2022, **7**, 2070–2078.
6 S. D. Poynton, R. C. T. Slade, T. J. Omasta, W. E. Mustain, R. Escudero-cid and J. R. Varcoe, *J. Mater. Chem.*, 2014, **2**, 5124–5130.
7 C. He, A. C. Yang-Neyerlin and B. S. Pivovar, *J. Electrochem. Soc.*, 2022, **169**, 024507.
8 S. Gottesfeld, D. R. Dekel, M. Page, C. Bae, Y. Yan, P. Zelenay and Y. S. Kim, *J. Power Sources*, 2018, **375**, 170–184.
9 D. R. Dekel, *J. Power Sources*, 2017, **2018**, 158–169.
10 M. Adamski, T. J. G. Skalski, B. Britton, T. J. Peckham, L. Metzler and S. Holdcroft, *Angew. Chem., Int. Ed.*, 2017, **6**, 9186–9189.
11 Z. Long, J. Miyake and K. Miyatake, *ACS Appl. Energy Mater.*, 2019, **2**, 7527–7534.
12 D. Yazili, E. Marini, T. Saatkamp, A. Münchinger, T. de Wild, L. Gubler, G. Titvinidze, M. Schuster, C. Schare, L. Jörissen and K. D. Kreuer, *J. Power Sources*, 2023, **563**, 23791–23799.
13 A. D. Mohanty, S. E. Tignor, J. A. Krause, Y. K. Choe and C. Bae, *Macromolecules*, 2016, **49**, 3361–3372.
14 S. Noh, J. Y. Jeon, S. Adhikari, Y. S. Kim and C. Bae, *Acc. Chem. Res.*, 2019, **52**, 2745–2755.
15 E. J. Park and Y. S. Kim, *J. Mater. Chem. A*, 2018, **6**, 15456–15477.
16 J.-S. Wang and K. Matyjaszewski, *Macromolecules*, 1995, **28**, 7901–7910.
17 J. Chiefari, Y. K. Chong, F. Ercole, J. Krstina, J. Jeffery, T. P. T. Le, R. T. A. Mayadunne, G. F. Meijs, C. L. Moad, G. Moad, E. Rizzardo and S. H. Thang, *Macromolecules*, 1998, **31**, 5559–5562.
18 G. Moad and E. Rizzardo, *Macromolecules*, 1995, **28**, 8722–8728.
19 D. Breslow and N. Newburg, *J. Am. Chem. Soc.*, 1057, **20**, 5072–5073.
20 W. You, K. J. T. Noonan and G. W. Coates, *Prog. Polym. Sci.*, 2020, **100**, 101177.
21 M. G. Marino and K. D. Kreuer, *ChemSusChem*, 2015, **8**, 513–523.
22 M. R. Sturgeon, C. S. Macomber, C. Engtrakul, H. Long and B. S. Pivovar, *J. Electrochem. Soc.*, 2015, **162**, 366–372.
23 H. Long, K. Kim and B. S. Pivovar, *J. Phys. Chem. C*, 2012, **116**, 9419–9426.
24 F. Gu, H. Dong, Y. Li, Z. Sun and F. Yan, *Macromolecules*, 2014, **47**, 6740–6747.
25 L. Gu, H. Dong, Z. Sun, Y. Li and F. Yan, *RSC Adv.*, 2016, **6**, 94387–94398.
26 B. Zhang, H. Long, R. B. Kaspar, J. Wang, S. Gu, Z. Zhuang, B. Pivovar and Y. Yan, *RSC Adv.*, 2018, **8**, 26640–26645.
27 C. T. Womble, J. Kang, K. M. Hugar, W. Coates, S. Bernhard and K. J. T. Noonan, *Organometallics*, 2017, **36**, 4038–4046.
28 B. Xue, X. Dong, Y. Li, J. Zheng, S. Li and S. Zhang, *J. Membr. Sci.*, 2017, **537**, 151–159.

 This journal is © The Royal Society of Chemistry 2024

Published on 16 May 2024. Downloaded on 3/7/2026 1:23:47 AM.

29 H. Long and B. Pivovar, *J. Phys. Chem. C*, 2014, **118**, 9880–9888.
30 A. G. Wright, T. Weissbach and S. Holdcroft, *Angew. Chem., Int. Ed.*, 2016, **55**, 4818–4821.
31 O. D. Thomas, K. J. W. Y. Soo, T. J. Peckham, M. P. Kulkarni and S. Holdcroft, *J. Am. Chem. Soc.*, 2012, **134**, 34.
32 J. Fan, A. G. Wright, B. Britton, T. Weissbach, T. J. G. Skalski, J. Ward, T. J. Peckham and S. Holdcroft, *ACS Macro Lett.*, 2017, **6**, 1089–1093.
33 K. M. Hugar, H. A. Kostalik and G. W. Coates, *J. Am. Chem. Soc.*, 2015, **137**, 8730–8737.
34 J. Fan, S. Willdorf-Cohen, E. M. Schibli, Z. Paula, W. Li, T. J. G. Skalski, A. T. Sergeenko, A. Hohenadel, B. J. Frisken, E. Magliocca, W. E. Mustain, C. E. Diesendruck, D. R. Dekel and S. Holdcroft, *Nat. Commun.*, 2019, **10**, 2306–2316.
35 C. G. Arges, J. Parrondo, G. Johnson, A. Nadhan and V. Ramani, *J. Mater. Chem.*, 2012, **22**, 3733–3744.
36 Z. Sun, B. Lin and F. Yan, *ChemSusChem*, 2018, **11**, 58–70.
37 J. Wang, S. Gu, R. Kaspar, B. Zhang and Y. Yan, *ChemSusChem*, 2013, **6**, 2079–2082.
38 M. Moreno-González, P. Mardle, S. Zhu, B. Gholamkhass, S. Jones, N. Chen, B. Britton and S. Holdcroft, *J. Power Sources Adv.*, 2023, **19**, 100109–100120.
39 K. M. Hugar, W. You and G. W. Coates, *ACS Energy Lett.*, 2019, **4**, 1681–1686.
40 T. Weissbach, A. G. Wright, T. J. Peckham, A. Sadeghi Alavijeh, V. Pan, E. Kjeang and S. Holdcroft, *Chem. Mater.*, 2016, **28**, 8060–8070.
41 J. E. Mark, in *The Physical Properties of Polymers Handbook*, ed. J. E. Mark, Springer NY, New York, 2nd edn, 2007.
42 A. L. G. Biancolli, A. Konovalova, E. I. Santiago and S. Holdcroft, *Int. J. Electrochem. Sci.*, 2023, **18**, 100288–100298.
43 E. M. Schibli, J. C. Stewart, A. A. Wright, B. Chen, S. Holdcroft and B. J. Frisken, *Macromolecules*, 2020, **53**, 4908–4916.
44 K. Kreuer and P. Jannasch, *J. Power Sources*, 2018, **375**, 361–366.
45 X. Wang, J. P. McClure and P. S. Fedkiw, *Electrochim. Acta*, 2012, **79**, 126–132.
46 Y. S. Li, T. S. Zhao and W. W. Yang, *Int. J. Hydrogen Energy*, 2010, **35**, 5656–5665.